





## Experimental exploration of dynamic phase transitions and associated metamagnetic fluctuations for materials with different Curie temperatures

J. M. Marín Ramírez <sup>1,2</sup>, E. Oblak,<sup>1</sup> P. Riego,<sup>1,3</sup> G. Campillo <sup>4</sup>, J. Osorio <sup>2</sup>, O. Arnache,<sup>2</sup> and A. Berger <sup>1</sup>

<sup>1</sup>*CIC nanoGUNE BRTA, 20018 Donostia – San Sebastián, Spain*

<sup>2</sup>*Instituto de Física, Facultad de Ciencias Exactas y Naturales, Universidad de Antioquia, Apartado Aéreo 1226, Medellín, Colombia*

<sup>3</sup>*Departamento de Física de la Materia Condensada, Universidad del País Vasco (UPV/EHU), 48080 Bilbao, Spain*

<sup>4</sup>*Facultad de Ciencias Básicas, Universidad de Medellín, Medellín, Colombia*



(Received 17 April 2020; accepted 28 July 2020; published 20 August 2020)

We study dynamic magnetic behavior in the vicinity of the dynamic phase transition (DPT) for a suitable series of samples that have different Curie temperatures  $T_C$ , which thus enables us to experimentally explore the role of the reduced temperature  $T/T_C$  in the DPT. For this purpose, we fabricate  $\text{Co}_{1-x}\text{Ru}_x$  epitaxial thin films with uniaxial in-plane anisotropy by means of sputter deposition in the concentration range  $0.0 \leq x \leq 0.26$ . All samples are ferromagnetic at room temperature, exhibit an abrupt magnetization reversal along their easy axis, and represent a unique  $T_C$  and thus  $T/T_C$  ratio according to their Ru concentration. The dynamic magnetic behavior is measured by using an ultrasensitive transverse magneto-optical detection method and the resulting dynamic states are explored as a function of the applied magnetic field amplitude  $H_0$  and period  $P$ , as well as an additional bias field  $H_b$ , which is the conjugate field of the dynamic order parameter  $Q$ . Our experimental results demonstrate that the qualitative behavior of the dynamic phase diagram is independent of the  $T/T_C$  ratio and that for all  $T/T_C$  values we observe metamagnetic anomalies in the dynamic paramagnetic state, which do not exist in the corresponding thermodynamic phase diagram. However, quantitatively, these metamagnetic anomalies are very strongly dependent on the  $T/T_C$  ratio, leading to an about 20-fold increase of large metamagnetic fluctuations in the paramagnetic regime as the  $T/T_C$  ratio increases from 0.37 to 0.68. Also, the phase space range in which these anomalous metamagnetic fluctuations occur extends closer and closer to the critical point as  $T/T_C$  increases.

DOI: [10.1103/PhysRevE.102.022804](https://doi.org/10.1103/PhysRevE.102.022804)

### I. INTRODUCTION

Nonequilibrium phenomena and their dynamic behavior represent a topic of currently growing interest. In particular, the phenomenon of dynamic phase transition (DPT) has been explored in different fields and has enabled an understanding of the complexity of dynamic responses for a wide variety of systems. Examples of such studies can be found in biological and chemical systems [1,2], statistical processes applied to social human activity [3,4], time evolution of magnetic properties in promising materials such as nanographene [5], and quantum dynamics [6], among others. Nevertheless, today's understanding of experimental and theoretical aspects of nonequilibrium phenomena is far inferior to the understanding of its equilibrium counterpart [7]. The study of DPTs in magnetic or general spin systems has been primarily pursued by means of theoretical and modeling approaches [7–15], in comparison to rather few experimental works that conducted detailed explorations of the nature of DPTs [16–18], even if the frequency dependence of hysteresis loops has been explored for a long time, including in studies of thin films [19–21]. This mismatch is mainly related to the very specific conditions that must be fulfilled to experimentally explore DPTs, which not only need measurement setups with extremely high sensitivity, but more relevantly require special sample designs, as we will discuss later in conjunction with

the specific sample series that we employ in our study here [16–18].

From basic thermodynamics, it is well known that equilibrium magnetic systems can undergo thermodynamic phase transitions (TPTs), as seen in Fig. 1(a). At a TPT (black line ending at the red circle in Fig. 1(a), which indicates the critical point) the system's magnetization  $M$  changes in a nonanalytical manner as a function of temperature or external magnetic field, to which the system is subjected [22,23]. Specifically, the magnetic system is characterized by an intrinsic critical temperature  $T_C$ , at which  $M$  vanishes in the absence of an applied field. Therefore,  $T_C$  separates two different regimes, the ordered state or ferromagnetic (FM) phase ( $T < T_C$ ) and the disordered or paramagnetic (PM) phase ( $T > T_C$ ) [24,25]. From Fig. 1(a) it is noticeable that in the FM phase, there is a field-dependent first-order phase transition as shown by the black solid line. Likewise, under the influence of a time-dependent oscillating external field  $H(t)$ , bistable magnetic systems (in which the magnetization switches between two stable states, i.e.,  $\pm M_s$ ) can undergo a qualitative change in their dynamic magnetic response. From Fig. 1(b) we can see that these variations lead to a dynamic phase transition, which also ends in a critical point that is now characterized by a particular critical period  $P_C$ , which separates the ordered dynamic FM phase ( $P < P_C$ ) from the disordered dynamic PM phase ( $P > P_C$ ) [7–10].

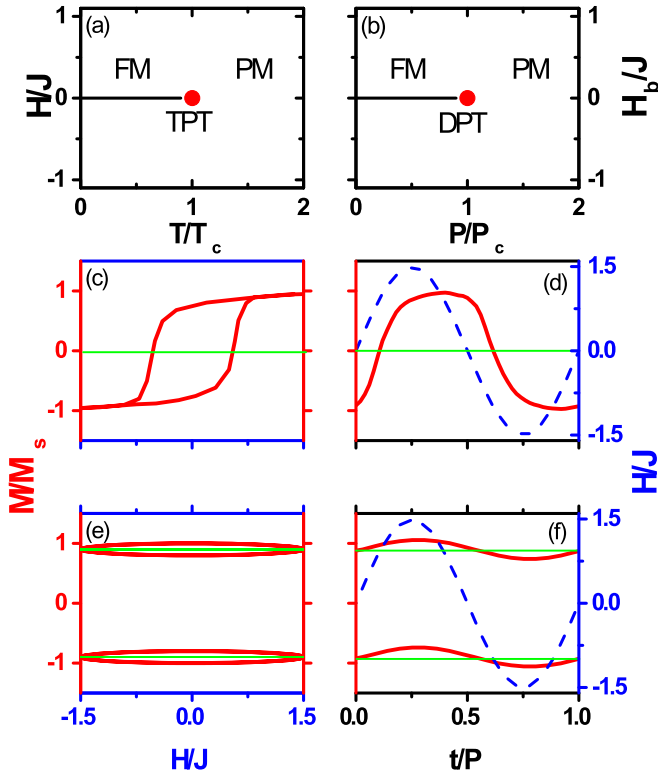


FIG. 1. Plots of the (a) TPT and (b) DPT phase diagrams. In both diagrams, the red circle represents the critical point, which separates the ferromagnetic and paramagnetic phases. The horizontal black line stands for the phase boundary within the FM state, at which a first-order phase transition occurs. Also shown are schematic illustrations of  $M/M_S$  vs  $H$  hysteresis loops (red lines) for two different field periods representing (c) the PM phase and (e) the FM phase. In (d) and (f) the red line represents the  $M(t)$  response in comparison to the time-dependent field (blue dashed line). The solid green lines in (c)–(f) all indicate the time-averaged magnetization values representing the order parameter  $Q$ .

For simplicity, we assume here that  $H(t)$  has a sinusoidal form, i.e.,  $H(t) = H_0 \sin(\frac{2\pi}{P}t)$ . Then  $H_0$  is the field amplitude, while  $P$  is the oscillation period of the external field ( $P = \frac{2\pi}{\omega}$ ). As the period of  $H(t)$  changes, so does the magnetization response in terms of the time-dependent magnetization  $M(t)$ , which is the system-averaged spin expectation value at any given time. Then the overall dynamic behavior can be described by using the time-averaged magnetization of the system [11–14]

$$Q = \frac{1}{P} \int_0^P M(t) dt, \quad (1)$$

which was identified as the dynamic order parameter [26].<sup>1</sup> When the applied field oscillation is slow and correspondingly

<sup>1</sup>The commonly used definition of Eq. (1) is a simplification for the case where only one component of the magnetization is relevant. In general, of course,  $M$  is a three-dimensional vector and accordingly  $Q$  is a three-dimensional vector as well. This fact has been mostly ignored in the literature, but it is the focus of a recently concluded study by some of us [27].

its  $P$  significantly larger than the critical period  $P_C$ ,  $M(t)$  can be almost fully inverted [Fig. 1(c)] so that the net magnetization averaged over one full field cycle is zero, i.e.,  $Q = 0$  [green solid line in Figs. 1(c) and 1(d)]. Therefore, as indicated in Fig. 1(d) for  $P > P_C$ , the time-dependent magnetization (red line) of the system can follow the external excitation  $H(t)$  (blue dotted line) with only a slight delay. As the external field period becomes smaller, there is a point at which the magnetization response cannot follow the external field excitation anymore, which leads to a spontaneous symmetry breaking of the hysteresis loop for  $P < P_C$  and causes a nonzero average value of the magnetization, as schematically illustrated in Fig 1(e). The figure also demonstrates that in this dynamic regime, two separate stable dynamic trajectories exist, which are also visible in Fig. 1(f). For both of these trajectories, the net magnetization averaged over an entire cycle becomes different from zero, as symbolized by the green lines in Figs. 1(e) and 1(f). Which one of these equivalent states the system will occupy depends hereby on the history of the dynamic system in the same way in which the equilibrium magnetization in remanence depends on the applied field history [17].

Consistent with these observations, the time-averaged magnetization value  $Q$  as the dynamic order parameter changes from zero to a nonzero value in a continuous fashion at a distinctive period  $P = P_C$ , meaning that at that point a second-order dynamic phase transition takes place [15]. For  $P < P_C$  the system is in a dynamically ordered state or dynamic FM phase with  $Q \neq 0$ , whereas for  $P > P_C$  the system exhibits a dynamically disordered state or dynamic PM phase where  $Q = 0$  [14,15]. The presence of a small time-independent bias field  $H_b$ , applied in addition to the oscillatory field, extends the overall phase space due to the fact that  $H_b$  is found to be the conjugate field associated with the order parameter  $Q$  in the same manner in which the applied field  $H$  is the conjugate field for  $M$  in the thermodynamic phase space [16,17]. The dynamic phase diagram [Fig. 1(b)] shows that as  $H_b$  changes its sign, it induces a first-order phase transition (black horizontal line) between different dynamically ordered states in the FM phase ( $P < P_C$ ). This was first observed in an experimental study [17], which also demonstrated the occurrence of hysteresis in the  $Q$  vs  $H_b$  dependence that is associated with a first-order dynamic phase transition. Thus, at first glance the dynamic order parameter  $Q$  seems to mimic the behavior of  $M$  in thermal equilibrium very closely.

A simple but powerful approach to describe the nature of DPTs theoretically was first introduced by Tomé and de Oliveira [26]. By means of a mean-field approach, they computed the evolution of the kinetic Ising model (KIM) [28–31] under the assumption of Glauber stochastic transition probabilities [32]. In this approach, the corresponding time-dependent Hamiltonian can be written in the form

$$\mathcal{H} = -\mathcal{J} \sum_{[i,j]} S_i S_j - H(t) \sum_i S_i. \quad (2)$$

The first term represents the exchange energy of the spin system with  $\mathcal{J} > 0$  being the ferromagnetic exchange coupling constant and  $S_i$  the Ising spin at location  $i$ , which can

take only two possible values  $\pm 1$ . The sum  $\sum_{[i,j]}$  runs over all exchange coupled sites. The second term corresponds to the Zeeman energy associated with an external magnetic field that is spatially uniform for all spins sites  $i$  but time-dependent  $H(t)$ . Thus, it is this energy term that drives dynamic changes due to its explicit time dependence. It was especially these types of KIM calculations that demonstrated very relevant similarities in between dynamic and thermodynamic order states and phase transitions, including identical values for critical exponents [33–37]. Nevertheless, not all aspects of TPTs seem to be replicated in dynamic phenomena or vice versa. Specifically, the impact of surfaces on phase transitions appears to be far different in dynamic ordering phenomena than in equilibrium physics [34,37,38]. Also, recent experiments for thin Co films have led to the observation of anomalous fluctuations in the PM dynamic phase that do not exist in thermal equilibrium [18]. This behavior occurs for sufficiently large  $H_b$  values in the PM phase and can be attributed to metamagnetic tendencies, which imply a rather sharp increase of  $Q$  in a small range of applied bias fields without going through an actual phase transition. Later, theoretical works confirmed these tendencies [39,40], which illustrates the important interplay in between theoretical and experimental work in this field of study.

Prior experimental findings have already indicated the type of sample that is needed to successfully detect the DPT and explore the associated dynamic phase space [16–18]. Specifically, magnetic bistability of the sample must exist even on the macroscopic scale so that thin film systems with strong in-plane uniaxial anisotropy are the most suitable. This is primarily due to the vanishingly small magnetostatic effects that are present in these types of samples and thus mimic the fact that in virtually all theoretical studies, magnetostatic interactions are simply neglected [9,15,34–38,41–47]. Samples with these characteristics have been previously fabricated. In particular, Co-based thin films have been successfully utilized and we follow a similar strategy here as outlined in Sec. II A [16–18,20,48–55].

Despite their overall success in exploring relevant dynamic behavior, all experimental studies of DPTs so far have been limited to low  $T/T_C$  ratios only. As a result, the impact of  $T/T_C$  on the DPT and the general phase space behavior has not been explored, and thus experimental knowledge is still very limited to date. This constitutes a truly problematic knowledge gap, because also the theoretical understanding of temperature effects is rather modest and more importantly has resulted in seemingly contradictory results in the past [8,11]. The reason why experimental studies have been limited to low  $T/T_C$  ratios so far is related to the fact that all detailed DPT experiments have been limited to room temperature (RT) measurements to achieve the required precise  $H(t)$  control and sensitive and fast  $M(t)$  detection, which are fundamental conditions for such experiments [16,17]. Given these experimental boundary conditions, it is actually much more straightforward to vary the  $T_C$  of magnetic systems while keeping the experimental measurement conditions for DPT studies constant. In addition, actual changes of  $T$  to vary  $T/T_C$  ratios, especially attempts to utilize temperature well above room temperature, could lead to structural changes or segregation processes due to atomic diffusion in magnetic

samples that might impact or alter experimental results of DPT observations.

Consequently, the goal of the present work is to experimentally study the impact of the  $T/T_C$  ratio on the DPT in ferromagnetic films and explore the associated phase space. For this purpose, we have chosen to fabricate a series of epitaxial single-crystal  $\text{Co}_{1-x}\text{Ru}_x(10\bar{1}0)$  thin film samples in the Ru concentration range of  $0 \leq x \leq 0.26$  as a suitable sample set to explore DPTs. Actually, in an earlier work we investigated the effect of Ru doping within  $\text{Co}_{1-x}\text{Ru}_x$  alloy thin films on magnetocrystalline anisotropy and we demonstrated that both the hcp crystal structure and epitaxial quality of such samples can be maintained and that the in-plane uniaxial nature of its static magnetic state is unaffected [54]. Furthermore, this study also demonstrated that  $T_C$  can be modified precisely and reproducibly as a function of the doping concentration [54,56]. Therefore, such thin films should be appropriate to study the role that  $T/T_C$  might play in the DPT and its associated phase space behavior while allowing us to keep the experimental measurement temperature constant at RT.

The layout of this paper is as follows. Following this introduction, sample preparation and structural and static magnetic characterization are presented in Sec. II A. Section II B introduces the experimental setup for the DPT measurements and associated phase space exploration and discusses the specific experimental conditions utilized. In Sec. III A, the main results of the observed dynamic behavior within the  $H_b$ - $P$  and  $H_b$ - $H_0$  phase spaces in the vicinity of the DPT are presented for different  $T/T_C$  ratios. A detailed quantitative evaluation of metamagnetic fluctuation is presented in Sec. III B. In Sec. IV we summarize and discuss the conclusions of our work.

## II. EXPERIMENTAL DETAILS

### A. Sample preparation and characterization

Epitaxial  $\text{Co}_{1-x}\text{Ru}_x(10\bar{1}0)$  thin films with Ru concentration  $x$  ranging from 0 to 0.26 were grown by cosputter deposition at room temperature in a pure 3-mTorr Ar atmosphere. To achieve epitaxy and this particular crystalline orientation, which contains the  $c$  axis in the surface plane and thus induces a macroscopic in-plane easy magnetization axis, a template bilayer composed of Ag(110) and Cr(211) was used, in accordance with prior work [51,54,55]. The overall growth sequence is illustrated in Fig. 2(a) and it includes a hydrofluoric acid etched Si(110) substrate, 37.5 nm of Ag(110), 10 nm of Cr(211), 20 nm of  $\text{Co}_{1-x}\text{Ru}_x(10\bar{1}0)$ , and on top of it a 10-nm  $\text{SiO}_2$  overcoat, which was deposited to avoid oxidation and contamination. The  $\text{Co}_{1-x}\text{Ru}_x(10\bar{1}0)$  thin film sample preparation was based on Ref. [54], but the therein utilized CrRu was not used for our study here, as it turned out not to be necessary to achieve a sufficiently high epitaxial quality.

To analyze and verify the sample quality, x-ray-diffraction measurements of all samples were performed at RT using the  $\theta$ - $2\theta$  configuration with Cu  $K_\alpha$  radiation ( $\lambda = 1.5406 \text{ \AA}$ ). Several exemplary diffractograms are presented in Fig. 2(b). From the data we observe a single sharp peak related to the  $\text{Co}_{1-x}\text{Ru}_x$  alloy film, which represents the  $(10\bar{1}0)$  surface orientation, and thus confirms the epitaxial nature of our films that exhibit an in-plane hcp  $c$  axis which corresponds to the

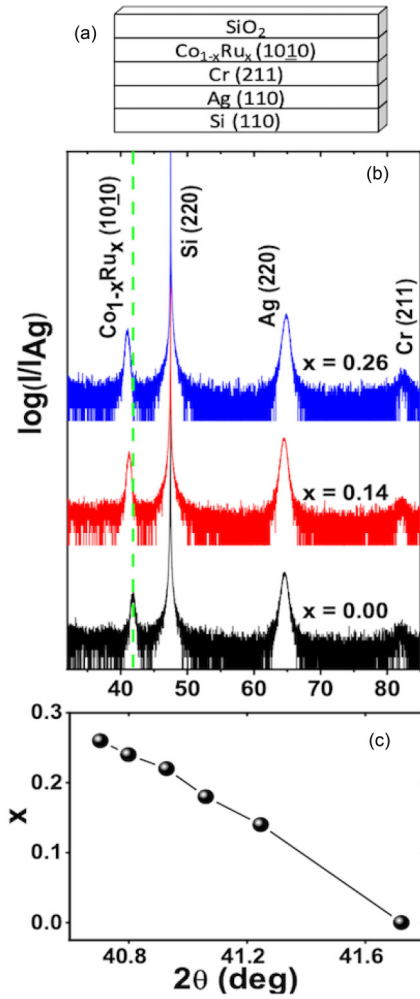


FIG. 2. (a) Schematics of the epitaxial  $\text{Co}_{1-x}\text{Ru}_x$  (1010) thin films, which were grown on a  $\text{Si}(110)/\text{Ag}(110)/\text{Cr}(211)$  template and coated by 10 nm of  $\text{SiO}_2$  to avoid oxidation. (b) X-ray-diffraction pattern for  $\text{Co}_{1-x}\text{Ru}_x$  (1010) films with  $x = 0.00, 0.14$ , and  $0.26$  Ru content. (c) Experimentally determined  $\text{Co}_{1-x}\text{Ru}_x$  (1010) peak positions as a function of Ru concentration  $x$ . The circles are the experimental data points and the line is a guide to the eye.

magnetic easy axis (EA). A close inspection of this diffraction peak for  $\text{Co}_{1-x}\text{Ru}_x$  (1010) also shows that as the Ru content increases a shift towards smaller diffraction angles occurs, which is specifically shown in Fig. 2(c) and was previously reported for the same type of samples [54]. All our samples were verified to be epitaxial with the crystallographic  $c$  axis in-plane and their crystallographic properties were observed to be similar in relation to the principal diffraction peak height and width. Thus, their magnetic anisotropy properties should be comparable and their overall magnetic properties representative of their specific  $T_C$  values, which is associated with each specific alloy composition.

To confirm the ferromagnetic nature and anisotropic behavior of the samples, quasistatic magnetic  $M$  vs  $H$  measurements were taken from  $\pm 2$  kOe at RT using a vibrating sample magnetometer (VSM). Additionally, the evolution of the saturation magnetization  $M_S$  against temperature was monitored using a superconducting quantum interference device VSM

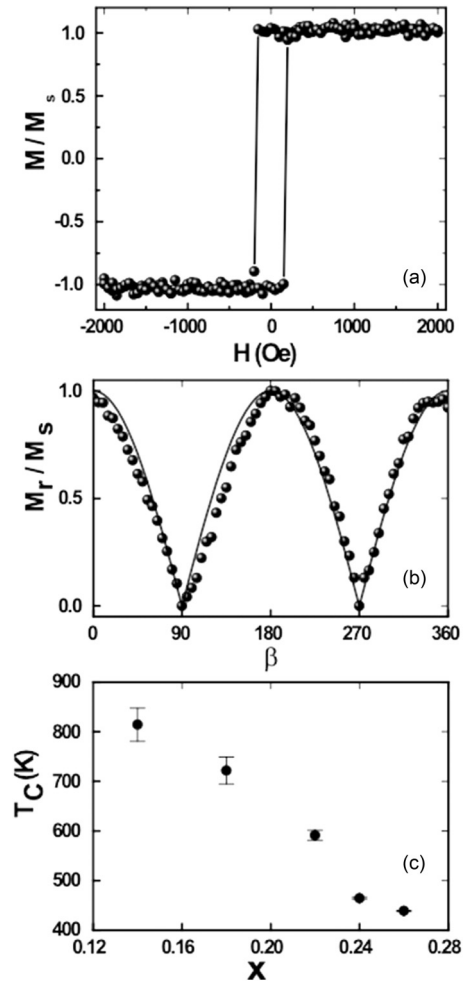


FIG. 3. (a) Hysteresis loop ( $M/M_S$  vs  $H$ ) measurement along the easy axis for a  $\text{Co}_{1-x}\text{Ru}_x$  ( $x = 0.24$ ) thin film sample with in-plane uniaxial anisotropy. (b) Angular dependence of the remanent magnetization  $M_r$ , normalized to the saturation magnetization  $M_S$ . The black circles are experimental data, while the black solid line represents the expected behavior for a highly anisotropic system. (c) Extrapolated Curie temperature values  $T_C$  for our  $\text{Co}_{1-x}\text{Ru}_x$  thin films as a function of Ru concentration  $x$ .

in the range 5–350 K. Figure 3(a) shows the normalized magnetization  $M/M_S$  as a function of the external magnetic field  $H$  measured along the in-plane EA for a  $\text{Co}_{1-x}\text{Ru}_x$  ( $x = 0.24$ ) thin film using the VSM. A squarelike loop was retrieved exhibiting a very sharp magnetization reversal<sup>2</sup> at the coercive field ( $\pm H_C$ ) that mimics the bistable nature of an Ising-like model, in which the magnetization switches between two stable states, i.e.,  $\pm M_S$  [16–18].

An exploration of the uniaxial in-plane anisotropy in our samples was examined by measuring the remanent

<sup>2</sup>Such quasistatic hysteresis loops are measured at a period that is orders of magnitude higher than the experimental conditions used for our DPT observations. Correspondingly, nucleated reversal domains actually have sufficient time to propagate through the entire sample in between two subsequent data points, making the hysteresis loop appear very abrupt, and thus suppress the dynamic behavior that defines the physics of dynamic phase transitions.

magnetization  $M_r$  as a function of the angle  $\beta$  (in reference to the EA orientation), at which an external magnetic field was initially applied within the surface plane to fully saturate the sample. The normalized remanent magnetization  $M_r/M_S$  is shown in Fig. 3(b) as a function of  $\beta$ . It is evident that for  $\beta = 0^\circ$  and  $180^\circ$ ,  $M_r/M_S$  is very close to 1, while for  $\beta = 90^\circ$  and  $270^\circ$ ,  $M_r$  nearly vanishes. Consequently, we have a  $180^\circ$  periodicity in the samples, which means that  $M_r/M_S$  is maximum when the external field  $H$  is applied along the EA direction, whereas this ratio is close to zero when applied along the magnetic hard axis. Our results agree very well with the analytical predictions of the Stoner-Wohlfarth model for a uniformly magnetized sample with uniaxial anisotropy [57], which is represented by the solid line in Fig. 3(b). For all other samples which are not displayed here, our VSM data look virtually identical. Consequently, they all exhibit textbook uniaxial in-plane anisotropy, even for their macroscopic sample-averaged behavior.

The evolution of the Curie temperature as a function of the Ru doping was analyzed by means of  $M$  vs  $T$  measurements along the EA for all our samples. Figure 3(c) presents the extrapolated  $T_C$  values determined by using the analytical expression proposed by Kuz'min [see Eq. (1) in Ref. [58]] to interpolate all measured  $M(T)$  data. As can be observed from these results, there is a clear decrease in  $T_C$  as the Ru content increases. This  $T_C$  reduction is similar to those reported in CoRu bulk samples and thin films, since Ru reduces the effective exchange coupling in these alloys [54,56,59]. The changing size of the error bars in Fig. 3(c) is attributed to the fact that for low Ru content we are extrapolating to temperatures far higher than our measured temperature range (5–350 K), while for high Ru content our measurement range is much closer to our samples' Curie temperatures.

We also need to address the fact that in order to change  $T/T_C$ , we are actually changing samples in our approach, which could lead to unintended consequences, as the DPT point is not fully identical in different samples. However, it would also not be identical if one were to use the same sample and vary  $T$  for the purpose of exploring the  $T/T_C$  dependence of DPT behavior. Usually, if one raises the temperature  $T$  of a magnetic system, its coercive field  $H_C$  decreases rather substantially, which is associated with the fact that in addition to larger thermal activation for higher  $T$ , the temperature-induced decrease in  $M$  (supporting a magnetization reversal via the Zeeman energy term) is less than the temperature-induced reduction in anisotropy energy (resisting a magnetization reversal) [60–62]. This means that if one were to conduct actual  $T$ -dependent measurements of the dynamic magnetic behavior and the DPT, one would have to compensate for a very significant  $H_C$  vs  $T$  shift in the data analysis. In our sample series,  $H_C$  is fairly constant as  $x$  and thus  $T/T_C$  are changed, because with increased  $x$  also the low-temperature saturation magnetization becomes much smaller, given the change in electronic structure associated with the changing compounds. Thus, magnetization and anisotropy changes with  $x$  nearly balance each other out, leading to only weak  $H_C$  vs  $x$  variations in our samples, which will aid our data analysis and reliability.

Thus, our  $\text{Co}_{1-x}\text{Ru}_x$  alloy thin films are highly oriented, exhibit ferromagnetism at RT, and have an in-plane uniaxial

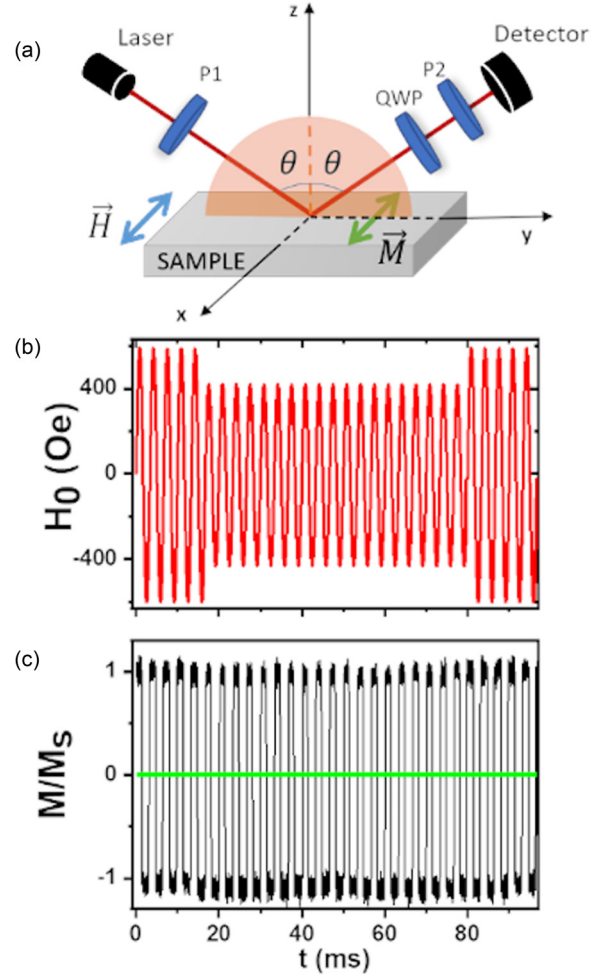


FIG. 4. (a) Experimental setup for an ultrasensitive TMOKE detection scheme which uses a coherent light source (laser), an initial polarizer (P1), a quarter waveplate, a second polarizer (P2), and a photodetector. (b) Applied field sequence with  $H_0 = 430$  Oe,  $H_b = 0$ , and  $P = 3.3$  ms. The first and last five cycles used a reference field amplitude  $H_{\text{ref}} = 580$  Oe to ensure full magnetization reversal in our samples. (c) Corresponding TMOKE signal trace for the  $\text{Co}_{0.76}\text{Ru}_{0.24}$  film samples, which shows full magnetization reversal throughout the sequence so that the time-averaged magnetization value  $\langle Q \rangle = 0$  (green solid line).

magnetic anisotropy. Furthermore, they exhibit systematically varying  $T_C$  values by means of Ru doping. Hence, we have generated a set of suitable test samples that will enable us to study dynamic magnetic behavior in the vicinity of the DPT [16–18] for different reduced temperatures  $T/T_C$  while allowing us to keep the experimental measurement temperature constant at RT.

## B. Experimental setup for dynamic magnetization measurements

Dynamic magnetization measurements to study the phase space in the vicinity of the DPT were carried out by using an ultrasensitive transversal magneto-optical Kerr effect (TMOKE) setup. A schematic of our experimental tool is depicted in Fig. 4(a), for which an ultralow-noise laser with  $\lambda =$

635 nm and 5-mW power output was used as a light source. The incident light coming from the laser passes through a fixed first polarizer (P1) set at a  $45^\circ$  angle, which establishes an about even mixture of *s* and *p* polarization, and then is reflected by the sample, which is positioned inside the gap of an electromagnet. The external field  $H(t)$  is applied transversally with respect to the incident plane of the light. The reflected beam goes through a rotatable quarter-waveplate (QWP) retarder and subsequently passes a second rotatable polarizer (P2). Finally, the transmitted light intensity is collected by a photodetector with built-in preamplifier. To limit the light intensity reaching the photodetector, coming from purely optically reflected light that does not carry magneto-optical signal information, QWP and P2 are rotated iteratively. After the point of minimum intensity has been identified, P2 is rotated by  $2^\circ$  away from this so-called extinction position, which provides experimental conditions that produce a large relative magneto-optical TMOKE signal, as well as sufficiently high light levels that can be easily detected with our photodetector. By using this specific experimental arrangement, our setup facilitates an effective polarization measurement for the TMOKE rather than a conventional intensity measurement, which enhances the detection sensitivity by about 2000%. Further details of this detection approach and its overall performance can be found in the literature [63,64]. Due to the high sensitivity of our TMOKE setup, time-resolved full hysteresis loop measurements can be recorded for periods of only 3.3 ms with excellent signal-to-noise ratio.

As already described in the Introduction,  $H_b$  is the conjugated field associated with  $Q$ . Correspondingly, small bias field amplitudes, even below  $\pm 2$  Oe, can induce large changes in the dynamic response [16,17]. Therefore, it is crucial that for entire measurement sequences, a high field stability in terms of amplitude and bias is ensured. Hence, we have implemented an iterative routine to minimize field fluctuations for  $H_0$  and  $H_b$ . This guarantees that  $H(t)$  is stable throughout the entire measurement process. In all our experiments, for  $H(t)$  periods in the range of 3.3–33.3 ms we have achieved field amplitude variations of less than  $\pm 1$  Oe for  $H_0$  amplitudes up to 600 Oe and bias field variations that are less than  $\pm 0.4$  Oe for all values of  $H_0$  and  $H_b$  that we utilized in this study. Both dynamic and static magnetic fields were applied using an electromagnet with minimal coercivity and low latency.

The magnetic field  $H(t)$  was applied in such a way that it is aligned with each sample's EA. This was done to detect full magnetization reversal once the field is strong enough to induce it in the sample. An example of the sinusoidal field  $H(t)$  used for our measurements is shown in Fig. 4(b). Here the overall period was set to  $P = 3.3$  ms with  $H_0 = 430$  Oe and without an applied bias field, i.e.,  $H_b = 0$ . Since we detect light intensity variations associated with the TMOKE, an appropriate calibration in between the measured light intensity  $I$  and its corresponding magnetization values must be established. For this purpose, a reference field  $H_{\text{ref}}$  sequence was used, which is larger in amplitude in comparison to  $H_0$  to ensure that the sample is fully saturated in each half cycle, and we induce a full magnetization reversal response in our films. Thus, we can correlate  $\pm M_S$  to the maximum (or minimum) intensity value and calibrate our measurements in this way. Another important function of  $H_{\text{ref}}$  is associated

with monitoring the stability of our experimental setup [16]. Correspondingly, this reference field sequence is applied at the beginning and at the end of each full dynamic measurement experiment, as illustrated by the first and last five cycles shown in Fig. 4(b). So, if any drifts occur during the measurement, a proper compensation routine can be implemented to correct such effects. A final consideration related to the reference measurement cycles is that the bias field is kept constant at  $H_b = 0$  to ensure that the order parameter is always equal to zero and both saturated states  $\pm M_S$  can be quantified with equal precision.

Figure 4(c) displays an example of the corresponding magneto-optical time traces measured by using our ultrasensitive TMOKE setup for the specific  $H(t)$  of Fig. 4(b). The normalized to  $M/M_S$  Kerr intensity data exhibit an almost squarelike behavior, meaning that when a field amplitude of  $H_0 = 430$  Oe is applied, the magnetization state switches back and forth from positive to negative saturation, just as in the case of the reference data at  $H_{\text{ref}} = 580$  Oe. Thus, even at  $H_0$ , we have a full reversal of the magnetization, so the cycle-averaged magnetization vanishes, i.e.,  $Q = 0$  (green solid line), and the system is in the dynamically PM state. These raw data also show that the signal-to-noise ratio is very good and the order parameter can be very precisely determined, even from a single field oscillation cycle, which is especially relevant for the accurate determination of higher-order observables, such as fluctuations.

### III. RESULTS AND DISCUSSION

#### A. Dynamic phase diagram exploration

Based upon the excellent stability achieved by our experimental setup and the textbooklike properties of our  $\text{Co}_{1-x}\text{Ru}_x$  alloy film series, we are now able to conduct a detailed exploration of the phase space in the vicinity of the DPT for different  $T/T_C$ . Figure 5 illustrates the bias field effect on the time-dependent magnetization response for the  $\text{Co}_{0.76}\text{Ru}_{0.24}$  thin film, which has a relatively high  $T/T_C$  ratio (approximately equal to 0.65) and a large magneto-optical signal. From Fig. 5(a) we can see that when  $H_b = 0$ , for a constant set of parameters ( $H_0$  and  $P$ ) the average order parameter  $\langle Q \rangle$  is equal to zero, displayed as a green solid line. When a small positive bias field ( $H_b = +5$  Oe) is applied while keeping  $H_0$  and  $P$  constant, the signal average becomes  $\langle Q \rangle \approx 1$  [green solid line in Fig. 5(b)]. Likewise, a small negative bias field ( $H_b = -5$  Oe) also causes a significant suppression of the time-dependent magnetization response and leads to  $\langle Q \rangle \approx -1$  [green solid line in Fig. 5(c)]. Thus, the system is in the paramagnetic dynamic regime, but rather modest values of  $H_b$  in comparison to  $H_0$  can induce large values of  $\langle Q \rangle$ . Hence, Fig. 5 confirms that this sample exhibits the distinct dynamic response expected for a system near its DPT. Furthermore, a close inspection of Figs. 5(b) and 5(c) shows that we applied a phase difference in between the two field sequences that were utilized to measure these curves. This is done in all our measurements to synchronize the bias field sign with the last reference field pulse so that any transient behavior can be relevantly suppressed. Thus, for positive values of  $H_b$  we start from a positively magnetized state, whereas for negative

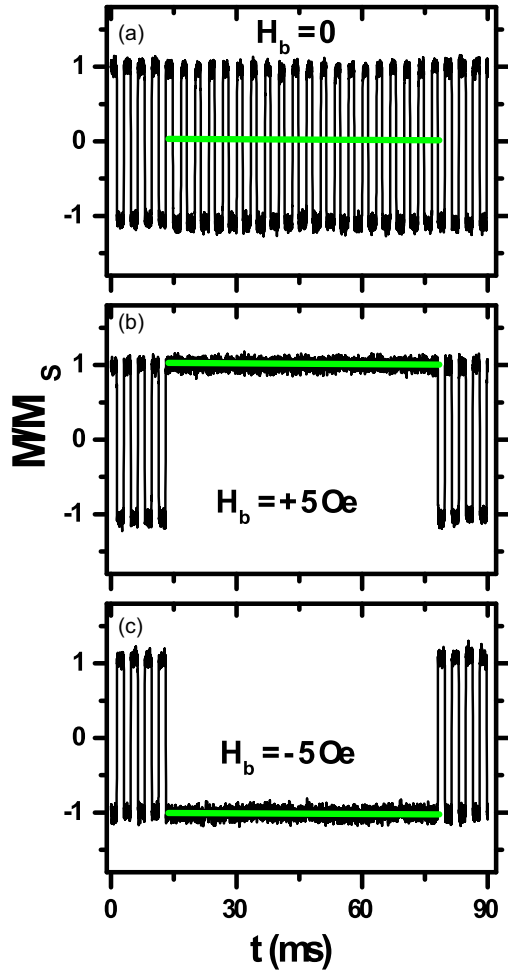


FIG. 5. The TMOKE signal traces representing  $M/M_S$  data for the same applied field  $H(t)$  sequence ( $P = 3.3$  ms,  $H_0 = 430$  Oe, and  $H_{\text{ref}} = 580$  Oe), except for the bias field, which is (a)  $H_b = 0$ , (b)  $H_b = +5$  Oe, and (c)  $H_b = -5$  Oe. The green solid lines represent the time-averaged magnetization values, which change as a function of  $H_b$ , producing (a)  $\langle Q \rangle = 0$ , (b)  $\langle Q \rangle \approx +1$ , and (c)  $\langle Q \rangle \approx -1$ .

values of  $H_b$ , the corresponding negatively magnetized state is initially populated. This synchronization in between the bias field and starting magnetic state is being done to minimize the transient time that is needed to achieve a stable dynamic sequence. For  $H_b \neq 0$  only one of the two possible dynamic states and associated  $M(t)$  sequences shown in Fig. 1(e) is dynamically stable, while the other one is metastable, generally leading to transient dynamic behavior, including a time-dependent  $Q$  vs  $H_b$  hysteresis [17]. Thus, by synchronizing the magnetic bias field and magnetic starting state we preselect a starting point that is close to the stable dynamic state and avoid the metastable dynamic state, which reduces transient dynamics and makes our measurements more efficient.

Figures 6(a) and 6(b) show experimental  $\langle Q \rangle$  data, which were measured using the field sequences presented in Fig. 4(b) for a fixed number of cycles, as a function of  $P$  and  $H_b$  as color-coded maps for different fixed field amplitudes, namely,  $H_0 = 428$  and 430 Oe, respectively. These specific field amplitudes were used here to measure the  $\langle Q \rangle(P, H_b)$  order parameter behavior in the  $P$ - $H_b$  phase space for a  $\text{Co}_{0.76}\text{Ru}_{0.24}$

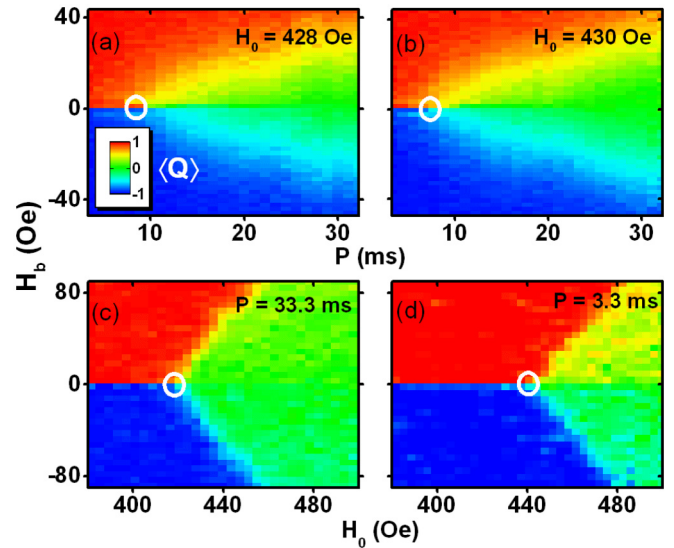


FIG. 6. Experimental  $\langle Q \rangle(P, H_b)$  data maps for (a)  $H_0 = 428$  Oe and (b)  $H_0 = 430$  Oe, measured for a  $\text{Co}_{0.76}\text{Ru}_{0.24}$  thin film, and experimental  $\langle Q \rangle(H_0, H_b)$  data maps for (c)  $P = 33.3$  ms and (d)  $P = 3.3$  ms for the same sample. Here  $P_C$  in (a) and (b) and  $H_{\text{crit}}$  in (c) and (d) are represented by the white circle. The color scale bar that is applicable for  $\langle Q \rangle$  in all graphs is shown in the inset in (a).

thin film. For all measurements, the reference field was set to 580 Oe. The color scale bar that is applicable for  $\langle Q \rangle$  in all graphs of Fig. 6 is shown as an inset in Fig. 6(a). The corresponding critical period  $P_C$  is visualized by the solid line circle in both figures. For both  $H_0$  amplitudes, we notice that there is a phase line at  $H_b = 0$  below  $P_C$  where the values or color of  $\langle Q \rangle$  abruptly changes from red ( $\langle Q \rangle \approx +1$ ) to blue ( $\langle Q \rangle \approx -1$ ), whereas for  $P > P_C$  this phase line is absent due to the nature of the paramagnetic dynamic phase. In this disordered state, there is a gradual change from  $\langle Q \rangle = 0$ , shown in green, towards  $\langle Q \rangle \neq 0$  as  $|H_b|$  increases, which is not associated with a dynamic phase transition [7, 15, 16]. These experimental measurements evidence that we can successfully detect dynamic phase transitions in our samples and map out the order parameter  $\langle Q \rangle(P, H_b)$  throughout the relevant phase space.

Another important experimental observation from Figs. 6(a) and 6(b) is that as the field amplitude  $H_0$  increases, an appreciable shift of the critical point  $P_C$  towards lower absolute  $P$  values occurs. In fact, the  $H_0$  dependence on  $P_C$  is rather strong, whereas the  $P$  dependence of the dynamic behavior is comparatively weaker. While we are changing  $P$  by one order of magnitude (3.3–33.3 ms) to explore the phase space that is visible in both figures, the very small change in the field amplitude  $H_0$  of less than 0.5% modifies the dynamic response in its absolute position quite substantially. Hence, Figs. 6(a) and 6(b) demonstrate that a  $P$ -dependent study is very suitable to explore fine details of the phase space near  $P_C$  [7]. However, if one would like to explore a larger portion of the dynamic phase space,  $P$ -dependent measurements are not particularly suitable, because  $P$  would have to change over many orders of magnitude while keeping all other conditions exactly constant, which is excessively problematic in any experiment. Consequently, it is much more practical from

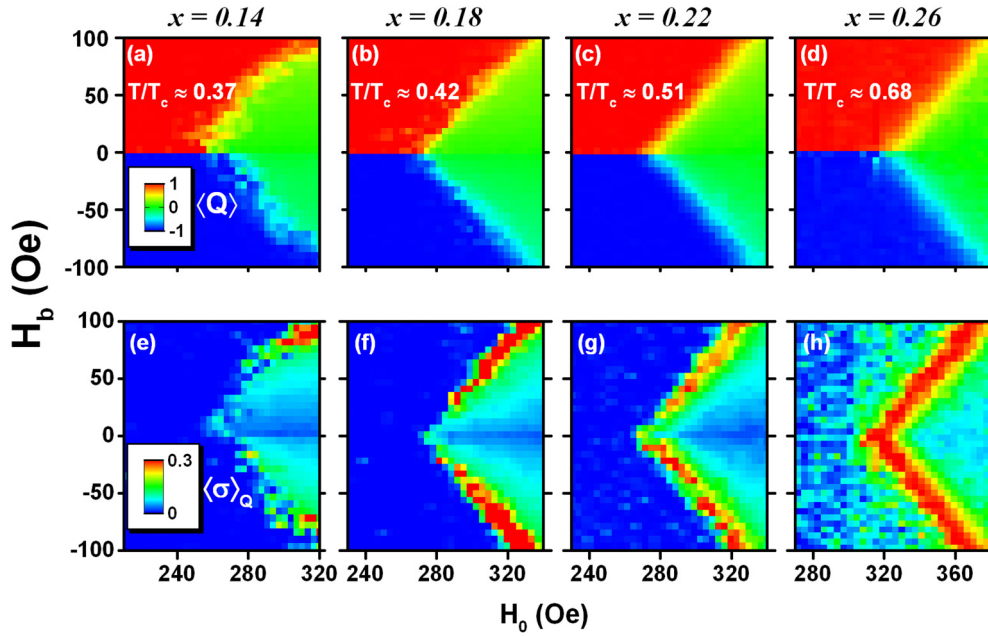


FIG. 7. Experimental phase space maps measured at  $P = 3.3$  ms: (a)–(d) dynamic order parameter  $\langle Q \rangle(H_0, H_b)$  and (e)–(h) fluctuations  $\langle \sigma \rangle_Q(H_0, H_b)$  for different  $\text{Co}_{1-x}\text{Ru}_x$  thin films with  $x = 0.14, 0.18, 0.22,$  and  $0.26$ , correspondingly representing different  $T/T_C$  ratios. Color scale bars for  $\langle Q \rangle$  and  $\langle \sigma \rangle_Q$  are located as insets in (a) and (e), respectively.

an experimental point of view to study the order parameter as a function of  $H_0$  and  $H_b$  for fixed frequencies. Such an approach will enable a wide range phase space exploration and correspondingly enable us to investigate the  $T/T_C$  dependence of dynamic magnetization behavior in such a wider phase space surrounding the critical point, which is our main goal. Therefore, we have measured  $\langle Q \rangle(H_0, H_b)$  order parameter maps as a function of the amplitudes of  $H_0$  and  $H_b$  while keeping the period of  $H(t)$  constant for all our  $\text{Co}_{1-x}\text{Ru}_x$  alloy thin films.

Figures 6(c) and 6(d) show such  $\langle Q \rangle(H_0, H_b)$  phase space data for fixed periods of  $P = 33.3$  and  $3.3$  ms, respectively, using once again the  $\text{Co}_{0.76}\text{Ru}_{0.24}$  sample. In both phase diagrams, we observe a well-defined phase line at  $H_b = 0$  that is associated with a first-order phase transition for  $H_0$  values below a critical threshold  $H_{crit}$  (encircled by the white solid line), where  $\langle Q \rangle$  changes abruptly from red to blue and which is qualitatively identical to the behavior that is present in the  $\langle Q \rangle(P, H_b)$  phase space. Hence, for  $H_0 > H_{crit}$  the system is in the dynamic paramagnetic state, while for  $H_0 < H_{crit}$  the system exhibits a dynamic ferromagnetic state. As  $P$  decreases [Fig. 6(d)],  $H_{crit}$  moves to higher values of  $H_0$  as expected and consistent with the behavior seen in Figs. 6(a) and 6(b). Furthermore, Figs. 6(c) and 6(d) demonstrate that the relevant phase space can still be accessed in an  $H_0$ – $H_b$ -type measurement, even if  $P$  changes by an order of magnitude, demonstrating the experimental accessibility and robustness of this approach. Thus, given the advantages of exploring the  $H_0$ – $H_b$  phase space, we now exploit this type of measurement to investigate the  $T/T_C$  dependence of the DPT and the surrounding phase space.

Figures 7(a)–7(d) display  $\langle Q \rangle(H_0, H_b)$  maps for  $P = 3.3$  ms and different  $\text{Co}_{1-x}\text{Ru}_x$  alloy films representing four dif-

ferent  $T/T_C$  ratios.<sup>3</sup> The corresponding color scale bar for all maps is located on the left-hand side of Fig. 7(a). Here  $H_{ref}$  was kept constant at 580 Oe in all measurements and a suitable  $H_0$  range was utilized to compensate for the rather modest  $H_C$  increase associated with varying  $x$ . Those figures show that, independent of the  $T/T_C$  ratio, all samples show fundamentally a very similar behavior. Specifically, we find that below a certain critical value ( $H_0 < H_{crit}$ ) there is a phase line at  $H_b = 0$  which delimits two possible stable states, either  $\langle Q \rangle \approx +1$  (red) or  $\langle Q \rangle \approx -1$  (blue), depending on the sign of  $H_b$ . Above  $H_{crit}$  this phase line is absent and  $\langle Q \rangle$  takes values that are close or equal to zero (green region). Thus, a dynamic phase transition takes place at  $H_{crit}$  and this critical point delimits the ordered ( $H_0 < H_{crit}$ ) from the disordered ( $H_0 > H_{crit}$ ) state.

Additionally, in all paramagnetic phases ( $H_0 > H_{crit}$ ) that are visible in Fig. 7, there is a strong onset behavior in  $\langle Q \rangle$  vs  $H_b$  that would indicate a strong metamagnetic character of the PM phase occurring for all samples. This metamagnetic character specifically appears in sidebandlike segments of the phase space, where there is a steep change in  $\langle Q \rangle$  with  $H_b$ . These changes are not abrupt and not hysteretic either. Thus,

<sup>3</sup>All samples exhibit a saturation-type behavior of the  $M(t)$  oscillation amplitude for  $H_0$  field amplitudes that are sufficiently larger than  $H_{crit}$ , reflecting the fact that above a saturation value for  $H_0$  the sample magnetization reaches saturation in each and every half cycle of the applied field. Thus, a further increase of  $H_0$  no longer changes the  $M$  vs.  $t$  trajectory in any meaningful way and the  $M(t)$  oscillation amplitude remains constant. In our experiments, we have chosen an  $H_{ref}$  value larger than the  $H_0$  saturation value for all samples, so the observed dynamic behavior becomes completely independent of  $H_{ref}$ .



we observed a metamagneticlike susceptibility increase without going through an actual phase transition. This behavior occurs only in the disordered regime. Hence, these results are analogous to those previously reported experimentally and theoretically for the  $P-H_b$  phase space in the vicinity of the DPT [18,39,40].

### B. Quantitative evaluation of metamagnetic fluctuations

Given the ability of our  $\langle Q \rangle(H_0, H_b)$  measurement scheme to explore large areas of the dynamic phase space, we were able to examine the metamagnetic tendencies in detail as a function of  $T/T_c$ , by analyzing the fluctuation behavior of the order parameter  $\langle \sigma \rangle_Q = \sqrt{(\langle Q^2 \rangle - \langle Q \rangle^2)}$ . Figures 7(e)–7(h) present color-coded maps for  $\langle \sigma \rangle_Q$ . Here dark blue regions correspond to no or minimal fluctuations values, while the red-colored areas denote larger fluctuations of the order parameter  $Q$ . As expected, the order parameter is extremely stable in the FM state and fluctuations are basically nonexistent. In the dynamic PM phase space areas, however, substantial fluctuation values occur, especially where the  $\langle Q \rangle(H_0, H_b)$  data indicate a metamagnetic character. Thus, the areas of large fluctuations exhibit a sideband structure that has a symmetric geometry with respect to the  $H_b = 0$  line. From this observation, we can conclude that metamagnetic fluctuations reported previously for Co films [18] can be regarded as a general phenomenon of the paramagnetic dynamic phase, independent of the  $T/T_c$  ratio. Furthermore, we observe that as the  $T/T_c$  ratio increases an enhancement of these metamagnetic fluctuations occurs as shown by Figs. 7(e)–7(h). Also, high fluctuation values occur ever closer to the critical point for higher  $T/T_c$  ratios. Thus, for the highest  $T/T_c$  sample, the critical fluctuations at  $H_{\text{crit}}$  and  $H_b = 0$  and the metamagnetic fluctuations in the PM state actually coalesce, which they do not do for the other samples. In some sense, these results are not entirely surprising, as fluctuations should increase in general as one brings a magnetic system closer to its critical temperature.

It should also be mentioned that at the highest  $T/T_c$  ratio (approximately equal to 0.68) traces of  $\langle \sigma \rangle_Q \neq 0$  can be detected even in the FM region [Fig. 7(h)]. However, this is related to the fact that the magneto-optical response of the samples decreases considerably as we reach higher  $T/T_c$  ratios. This leads to a lower magneto-optical signal amplitude  $\Delta I/I$ , which makes the data noisier and hence more susceptible to exhibiting small fluctuation values within our current phase space, a fact that is not driven by the magnetization dynamics itself.

A quantitative analysis of the metamagnetic fluctuations was done by analyzing the probability density associated with  $\langle \sigma \rangle_Q$  values in a normalized window surrounding the critical point, having an extent of  $H_0/H_{\text{crit}}$  (from 0.85 to 1.15) and  $H_b/H_{\text{crit}}$  (from  $-0.35$  to  $0.35$ ). Such a normalized window was chosen to compensate for the modest shift and associated increase in  $H_{\text{crit}}$ , which is synchronous with a change in coercive field  $H_c$  as  $x$  is varied. Hence, histogram plots were used to visualize the relative significance of sufficiently large fluctuations in the selected phase space. The probability density representing our lowest  $T/T_c$  ratio (approximately equal to 0.37) sample is shown in Fig. 8(a) in comparison to the data for the highest  $T/T_c$  ratio (approximately equal

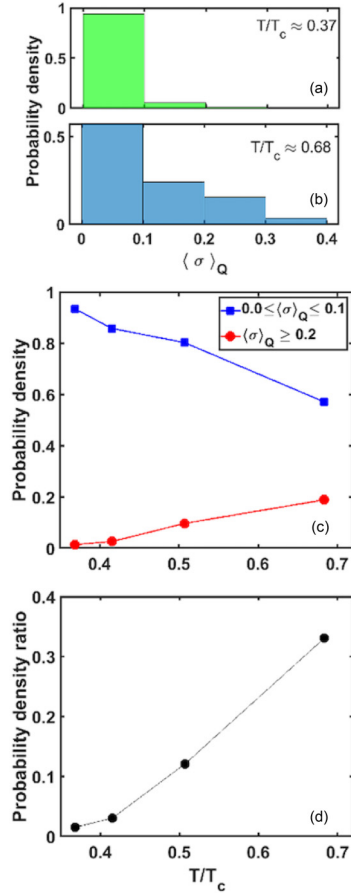


FIG. 8. Probability density histogram for the fluctuations at (a)  $T/T_c = 0.37$  ( $x = 0.14$ ) and (b)  $T/T_c = 0.68$  ( $x = 0.26$ ), (c) probability density values vs  $T/T_c$  for  $0.0 \leq \langle \sigma \rangle_Q \leq 0.1$  (blue squares) and  $\langle \sigma \rangle_Q \geq 0.2$  (red circles), and (d) probability density ratio evolution vs  $T/T_c$ .

to 0.68). It is noticeable that almost all existing fluctuations are rather weak ( $0.0 \leq \langle \sigma \rangle_Q \leq 0.1$ ) for the lowest  $T/T_c$  ratio. Thus, the probability for  $0.0 \leq \langle \sigma \rangle_Q \leq 0.1$  is almost equal to 1 and only very few larger fluctuations ( $\langle \sigma \rangle_Q > 0.1$ ) are recorded throughout the phase space. This is in agreement with previous results obtained for pure Co thin films, which represent an even lower  $T/T_c$  value than reported here. As the measurement temperature gets closer to  $T_c$ , a broader distribution of probability arises, as seen in Fig. 8(b). This fact is not related to the detection noise, previously mentioned in conjunction with Fig. 7(h), because this noise actually leads to small fluctuation values only. Instead, the broadened distribution in Fig. 8(b) represents a real dynamic state effect occurring for higher  $T/T_c$  values, namely, there is a larger portion of the phase space in which large fluctuations are present. Hence, the metamagnetic tendencies in the dynamic paramagnetic state are enhanced as the systems get closer to  $T_c$ . This fact is even more noticeable in Fig. 8(c), where we compared the probability to be in either a low fluctuation state ( $0.0 \leq \langle \sigma \rangle_Q \leq 0.1$ ) or a high fluctuation ( $\langle \sigma \rangle_Q \geq 0.2$ ) state. Here we observe that when the  $T/T_c$  ratio is low, the corresponding probability to have lower fluctuation values is high (blue squares) in contrast to higher fluctuation states

(red dots). As  $T/T_C$  increases, the dynamic states in the system are characterized by larger fluctuations, which are specifically associated with the metamagnetic character of the dynamic paramagnetic state. To visualize this fact very clearly, Fig. 8(d) shows the probability ratio  $P_{\text{high}}(\langle\sigma\rangle_Q \geq 0.2)/P_{\text{low}}(0.0 \leq \langle\sigma\rangle_Q \leq 0.1)$ , which shows a strong monotonic increase with  $T/T_C$  that represents an enhancement of large metamagnetic fluctuations by a factor of almost 22 as the  $T/T_C$  ratio doubles its value. Therefore, our experiments demonstrate unambiguously that the occurrence and extent of metamagnetic fluctuations are massively enhanced by increasing  $T/T_C$  of a magnetic system.

#### IV. CONCLUSION

In this work, we have conducted a comprehensive experimental study of dynamic magnetic states in the phase space surrounding the DPT as a function of the  $T/T_C$  ratio. For that purpose, we have fabricated a suitable set of  $\text{Co}_{1-x}\text{Ru}_x$  ( $0.0 \leq x \leq 0.26$ ) thin film samples that exhibit a Ru-concentration-dependent  $T_C$  so that the  $T/T_C$  ratio could be varied in our experimental study while keeping the measurement temperature  $T$  constant at room temperature, allowing us to take full advantage of our ultrasensitive TMOKE tool.

Our experimental study of the dynamic order parameter  $Q$  and related quantities was conducted by exploring the relevant phase space in two different ways, namely, by monitoring the dynamic state of our samples upon scanning either the  $(P, H_b)$  plane or the  $(H_0, H_b)$  plane. By using these alternative approaches, we demonstrated that  $P$ -dependent measurements, and thus  $(P, H_b)$ -plane observations, are primarily suitable to investigate fine details in the vicinity of the DPT. This is associated with the fact that the  $H_0$  sensitivity of  $P_C$  is rather strong, while the  $P$  dependence of the dynamic behavior is comparatively weak. Given that our goal was to study significant portions of the dynamic phase space, we pursued a  $(H_0, H_b)$ -plane phase space exploration in more detail in our study, and consequently  $\langle Q \rangle(H_0, H_b)$  maps were measured in detail to explore the  $T/T_C$  dependence of dynamic behavior.

Independent of  $T/T_C$ , all data sets exhibit the same main qualitative features of a dynamic phase transition, where at a unique  $P_C$  [in the  $(P, H_b)$  plane] or  $H_{\text{crit}}$  [in the  $(H_0, H_b)$  plane], a DPT takes place, which separates the ordered FM

dynamic regime from the disordered PM one. From our detailed experimental data, we can furthermore conclude that the metamagnetic fluctuations reported previously for magnetic thin films near the DPT [18,39,40] are observed to be a general phenomenon, which occurred in all samples and thus for all  $T/T_C$  ratios we studied. Therefore, the dynamic paramagnetic state is relevantly different from the equivalent equilibrium paramagnetic state of a conventional ferromagnet or spin system. A close inspection of the metamagnetic tendencies in the disordered PM regime, done by analyzing the fluctuation behavior of the order parameter  $\langle\sigma\rangle_Q$ , shows that significantly larger fluctuation values tend to appear as  $T/T_C$  increases, as seen in Figs. 7(e)–7(h). Also, these high fluctuation values occur ever closer to the critical point for sufficiently high  $T/T_C$  ratios, as the metamagnetic fluctuation regime appears to merge with the critical point, while this does not happen for low  $T/T_C$  values. A further analysis of the phase space probability density for  $\langle\sigma\rangle_Q$  showed that the occurrence of large fluctuation is becoming ever more likely with increasing  $T/T_C$ .

We hope that this work stimulates further experimental and theoretical studies of DPTs and their surrounding phase spaces by using the  $\langle Q \rangle(H_0, H_b)$  phase maps, which facilitate a wider inspection of the dynamic phase space behavior. Likewise, it would be interesting to develop an in-depth understanding of the importance of  $T/T_C$  ratios in general and specifically with respect to metamagnetic fluctuations, their size, their distribution, and their possible coalesce with the critical point.

#### ACKNOWLEDGMENTS

Work at nanoGUNE was supported by the Spanish Ministry of Science and Innovation under the Maria de Maeztu Units of Excellence Programme (Grant No. MDM-2016-0618) and Projects No. FIS2015-64519-R (MINECO/FEDER) and No. RTI2018-094881-B-100 (MCIU/Feder). J.M.M.R. acknowledges Colciencias for support through his Ph.D. fellowship. P.R. acknowledges “la Caixa” Foundation for support through her Ph.D. fellowship. O.A. and J.O. acknowledge financial support in the framework of the Solid-State Research group sustainability strategy (GES 2018-2019).

- 
- [1] M. Keskin and M. Ertaş, Frequency-dependent dynamic magnetic properties of the Ising bilayer system consisting of spin-3/2 and spin-5/2 spins, *Physica A* **496**, 79 (2018).
- [2] J. O. Dabiri, Landmarks and frontiers in biological fluid dynamics, *Phys. Rev. Fluids* **4**, 110501 (2019).
- [3] R. Shojaei, P. Manshour, and A. Montakhab, Phase transition in a network model of social balance with Glauber dynamics, *Phys. Rev. E* **100**, 022303 (2019).
- [4] B. Slavko, K. Glavatskiy, and M. Prokopenko, Dynamic resettlement as a mechanism of phase transitions in urban configurations, *Phys. Rev. E* **99**, 042143 (2019).
- [5] Y. Benhouria, I. Bouziani, I. Essaoudi, A. Ainane, and R. Ahuja, Quantum Monte Carlo study of dynamic magnetic properties of nano-graphene, *J. Magn. Magn. Mater.* **460**, 223 (2018).
- [6] P. Jurcevic, H. Shen, P. Hauke, C. Maier, T. Brydges, C. Hempel, B. P. Lanyon, M. Heyl, R. Blatt, and C. F. Roos, Direct Observation of Dynamical Quantum Phase Transitions in an Interacting Many-Body System, *Phys. Rev. Lett.* **119**, 080501 (2017).
- [7] P. Riego, P. Vavassori, and A. Berger, Towards an understanding of dynamic phase transitions, *Physica B* **549**, 13 (2018).
- [8] S. W. Sides, P. A. Rikvold, and M. A. Novotny, Kinetic Ising model in an oscillating field: Avrami theory for the hysteretic

- response and finite-size scaling for the dynamic phase transition, *Phys. Rev. E* **59**, 2710 (1999).
- [9] T. Yasui, H. Tutu, M. Yamamoto, and H. Fujisaka, Dynamic phase transitions in the anisotropic XY spin system in an oscillating magnetic field, *Phys. Rev. E* **66**, 036123 (2002).
- [10] K. Tauscher and M. Pleimling, Surface phase diagram of the three-dimensional kinetic Ising model in an oscillating magnetic field, *Phys. Rev. E* **89**, 022121 (2014).
- [11] B. K. Chakrabarti and M. Acharyya, Dynamic transitions and hysteresis, *Rev. Mod. Phys.* **71**, 847 (1999).
- [12] G. Korniss, C. J. White, P. A. Rikvold, and M. A. Novotny, Dynamic phase transition, universality, and finite-size scaling in the two-dimensional kinetic Ising model in an oscillating field, *Phys. Rev. E* **63**, 016120 (2000).
- [13] H. Jang and M. J. Grimson, Hysteresis and the dynamic phase transition in thin ferromagnetic films, *Phys. Rev. E* **63**, 066119 (2001).
- [14] M. Pleimling, Critical phenomena at perfect and non-perfect surfaces, *J. Phys. A: Math. Gen.* **37**, R79 (2004).
- [15] D. T. Robb, P. A. Rikvold, A. Berger, and M. A. Novotny, Conjugate field and fluctuation-dissipation relation for the dynamic phase transition in the two-dimensional kinetic Ising model, *Phys. Rev. E* **76**, 021124 (2007).
- [16] D. T. Robb, Y. H. Xu, O. Hellwig, J. McCord, A. Berger, M. A. Novotny, and P. A. Rikvold, Evidence for a dynamic phase transition in [Co/Pt]<sub>3</sub> magnetic multilayers, *Phys. Rev. B* **78**, 134422 (2008).
- [17] A. Berger, O. Idigoras, and P. Vavassori, Transient Behavior of the Dynamically Ordered Phase in Uniaxial Cobalt Films, *Phys. Rev. Lett.* **111**, 190602 (2013).
- [18] P. Riego, P. Vavassori, and A. Berger, Metamagnetic Anomalies near Dynamic Phase Transitions, *Phys. Rev. Lett.* **118**, 117202 (2017).
- [19] Y.-L. He and G.-C. Wang, Observation of Dynamic Scaling of Magnetic Hysteresis in Ultrathin Ferromagnetic Fe/Au(001) Films, *Phys. Rev. Lett.* **70**, 2336 (1993).
- [20] Q. Jiang, H.-N. Yang, and G.-C. Wang, Scaling and dynamics of low-frequency hysteresis loops in ultrathin Co films on a Cu(001) surface, *Phys. Rev. B* **52**, 14911 (1995).
- [21] J.-S. Suen and J. L. Erskine, Magnetic Hysteresis Dynamics: Thin  $p(1 \times 1)$  Fe Films on Flat and Stepped W(110), *Phys. Rev. Lett.* **78**, 3567 (1997).
- [22] M. E. Fisher and M. N. Barber, Scaling Theory for Finite-Size Effects in the Critical Region, *Phys. Rev. Lett.* **28**, 1516 (1972).
- [23] T. Wolfram, R. E. Dewames, W. F. Hall, and P. W. Palmberg, Surface magnetization near the critical temperature and the temperature dependence of magnetic-electron scattering from NiO, *Surf. Sci.* **28**, 45 (1971).
- [24] H. E. Stanley, *Introduction to Phase Transitions and Critical Phenomena* (Oxford University Press, New York, 1987).
- [25] J. M. Yeomans, *Statistical Mechanics of Phase Transitions* (Clarendon, Oxford, 1992).
- [26] T. Tomé and M. J. de Oliveira, Dynamic phase transition in the kinetic Ising model under a time-dependent oscillating field, *Phys. Rev. A* **41**, 4251 (1990).
- [27] M. Quintana, E. Oblak, J. M. Marín Ramírez, and A. Berger, Experimental exploration of the vector nature of the dynamic order parameter near dynamic magnetic phase transitions (unpublished).
- [28] M. Suzuki and R. Kubo, Dynamics of the Ising model near the critical point. I, *J. Phys. Soc. Jpn.* **24**, 51 (1968).
- [29] E. Stoll, K. Binder, and T. Schneider, Monte Carlo investigation of dynamic critical phenomena in the two-dimensional kinetic Ising model, *Phys. Rev. B* **8**, 3266 (1973).
- [30] H. Jang, M. J. Grimson, and T. B. Woolf, Stochastic dynamics and the dynamic phase transition in thin ferromagnetic films, *Phys. Rev. E* **70**, 047101 (2004).
- [31] M. F. Zimmer, Ising model in an oscillating magnetic field: Mean-field theory, *Phys. Rev. E* **47**, 3950 (1993).
- [32] R. J. Glauber, Time-dependent statistics of the Ising model, *J. Math. Phys.* **4**, 294 (1963).
- [33] S. W. Sides, P. A. Rikvold, and M. A. Novotny, Kinetic Ising Model in an Oscillating Field: Finite-Size Scaling at the Dynamic Phase Transition, *Phys. Rev. Lett.* **81**, 834 (1998).
- [34] H. Park and M. Pleimling, Surface Criticality at a Dynamic Phase Transition, *Phys. Rev. Lett.* **109**, 175703 (2012).
- [35] O. Idigoras, P. Vavassori, and A. Berger, Mean field theory of dynamic phase transitions in ferromagnets, *Physica B* **407**, 1377 (2012).
- [36] G. M. Buendía and P. A. Rikvold, Dynamic phase transition in the two-dimensional kinetic Ising model in an oscillating field: Universality with respect to the stochastic dynamics, *Phys. Rev. E* **78**, 051108 (2008).
- [37] H. Park and M. Pleimling, Dynamic phase transition in the three-dimensional kinetic Ising model in an oscillating field, *Phys. Rev. E* **87**, 032145 (2013).
- [38] P. Riego and A. Berger, Nonuniversal surface behavior of dynamic phase transitions, *Phys. Rev. E* **91**, 062141 (2015).
- [39] G. M. Buendía and P. A. Rikvold, Fluctuations in a model ferromagnetic film driven by a slowly oscillating field with a constant bias, *Phys. Rev. B* **96**, 134306 (2017).
- [40] X. Shi and P. Liu, Metamagnetic anomalies in the kinetic Ising model, *Physica A* **536**, 120998 (2019).
- [41] H. Fujisaka, H. Tutu, and P. A. Rikvold, Dynamic phase transition in a time-dependent Ginzburg-Landau model in an oscillating field, *Phys. Rev. E* **63**, 036109 (2001).
- [42] M. Acharyya, Nonequilibrium phase transition in the kinetic Ising model: Existence of a tricritical point and stochastic resonance, *Phys. Rev. E* **59**, 218 (1999).
- [43] S. Akkaya Deviren and E. Albayrak, Dynamic phase transitions in the kinetic Ising model on the Bethe lattice, *Phys. Rev. E* **82**, 022104 (2010).
- [44] B. Deviren, E. Kantar, and M. Keskin, Dynamic phase transitions in a cylindrical Ising nanowire under a time-dependent oscillating magnetic field, *J. Magn. Magn. Mater.* **324**, 2163 (2012).
- [45] B. O. Aktaş, Ü. Akıncı, and H. Polat, Critical phenomena in dynamical Ising-typed thin films by effective-field theory, *Thin Solid Films* **562**, 680 (2014).
- [46] Y. Yüksel, Monte Carlo study of magnetization dynamics in uniaxial ferromagnetic nanowires in the presence of oscillating and biased magnetic fields, *Phys. Rev. E* **91**, 032149 (2015).
- [47] R. Masrour, A. Jabar, A. Benyoussef, and M. Hamedoun, Critical phenomena in Ising-type thin films by Monte Carlo study, *J. Magn. Magn. Mater.* **403**, 167 (2016).

- [48] J. Brandenburg, R. Hühne, L. Schultz, and V. Neu, Domain structure of epitaxial Co films with perpendicular anisotropy, *Phys. Rev. B* **79**, 054429 (2009).
- [49] O. Idigoras, A. K. Suszka, P. Vavassori, B. Obry, B. Hillebrands, P. Landeros, and A. Berger, Magnetization reversal of in-plane uniaxial Co films and its dependence on epitaxial alignment, *J. Appl. Phys.* **115**, 083912 (2014).
- [50] V. Shukla, C. Mukherjee, R. Chari, S. Rai, K. S. Bindra, and A. Banerjee, Uniaxial magnetic anisotropy of cobalt thin films on different substrates using CW-MOKE technique, *J. Magn. Magn. Mater.* **370**, 100 (2014).
- [51] O. Idigoras, A. K. Suszka, P. Vavassori, P. Landeros, J. M. Porro, and A. Berger, Collapse of hard-axis behavior in uniaxial Co films, *Phys. Rev. B* **84**, 132403 (2011).
- [52] R. M. Thantirige, J. John, N. R. Pradhan, K. R. Carter, and M. T. Tuominen, Fabrication of flexible oriented magnetic thin films with large in-plane uniaxial anisotropy by roll-to-roll nanoimprint lithography, *J. Magn. Magn. Mater.* **407**, 273 (2016).
- [53] M. Kowalewski, C. M. Schneider, and B. Heinrich, Thickness and temperature dependence of magnetic anisotropies in ultra-thin fcc Co(001) structures, *Phys. Rev. B* **47**, 8748 (1993).
- [54] O. Idigoras, U. Palomares, A. K. Suszka, L. Fallarino, and A. Berger, Magnetic properties of room temperature grown epitaxial  $\text{Co}_{1-x}\text{Ru}_x$ -alloy films, *Appl. Phys. Lett.* **103**, 102410 (2013).
- [55] A. K. Suszka, O. Idigoras, E. Nikulina, A. Chuvilin, and A. Berger, Crystallography-Driven Positive Exchange Bias in Co/CoO Bilayers, *Phys. Rev. Lett.* **109**, 177205 (2012).
- [56] J. Crangle and D. Parsons, The magnetization of ferromagnetic binary alloys of cobalt or nickel with elements of the palladium and platinum groups, *Proc. R. Soc. London Ser. A* **255**, 509 (1960).
- [57] E. C. Stoner and E. P. Wohlfarth, A mechanism of magnetic hysteresis in heterogeneous alloys, *Philos. Trans. R. Soc. London Ser. A* **240**, 599 (1948).
- [58] M. D. Kuz'min, Shape of Temperature Dependence of Spontaneous Magnetization of Ferromagnets: Quantitative Analysis, *Phys. Rev. Lett.* **94**, 107204 (2005).
- [59] C. Eylich, A. Zamani, W. Huttema, M. Arora, D. Harrison, F. Rashidi, D. Broun, B. Heinrich, O. Mryasov, M. Ahlberg, O. Karis, P. E. Jönsson, M. From, X. Zhu, and E. Girt, Effects of substitution on the exchange stiffness and magnetization of Co films, *Phys. Rev. B* **90**, 235408 (2014).
- [60] W. C. Nunes, W. S. D. Folly, J. P. Sinnecker, and M. A. Novak, Temperature dependence of the coercive field in single-domain particle systems, *Phys. Rev. B* **70**, 014419 (2004).
- [61] E. Eftaxias and K. N. Trohidou, Numerical study of the exchange bias effects in magnetic nanoparticles with core/shell morphology, *Phys. Rev. B* **71**, 134406 (2005).
- [62] K.-D. Durst and H. Kronmüller, The coercive field of sintered and melt-spun NdFeB magnets, *J. Magn. Magn. Mater.* **68**, 63 (1987).
- [63] E. Oblak, P. Riego, L. Fallarino, A. Martínez-de-Guerenu, F. Arizti, and A. Berger, Ultrasensitive transverse magneto-optical Kerr effect measurements by means of effective polarization change detection, *J. Phys. D* **50**, 23LT01 (2017).
- [64] E. Oblak, P. Riego, A. Garcia-Manso, A. Martínez-de-Guerenu, F. Arizti, I. Artetxe, and A. Berger, Ultrasensitive transverse magneto-optical Kerr effect measurements using an effective ellipsometric detection scheme, *J. Phys. D* **53**, 205001 (2020).